Original Article

Institution of MECHANICAL ENGINEERS
Journal of MECHANICAL ENGINEERING SCIENCE

Proc IMechE Part C:
J Mechanical Engineering Science
0(0) 1–11

DOI: 10.1177/0954406217695847
journals.sagepub.com/home/pic
SAGE

Impact of nonlinear thermal radiation on stagnation-point flow of a Carreau nanofluid past a nonlinear stretching sheet with binary chemical reaction and activation energy

A Zaib[1], MM Rashidi[2], AJ Chamkha[3] and NF Mohammad[4]

Abstract

This research peruses the characteristics of nanoparticles on stagnation point flow of a generalized Newtonian Carreau fluid past a nonlinear stretching sheet with nonlinear thermal radiation. The process of mass transfer is modeled using activation energy and binary chemical reaction along with the Brownian motion and thermophoresis. For energy activation a modified Arrhenius function is invoked. With regard to the solution of the governing differential equations, suitable transformation variables are used to obtain the system of nonlinear ordinary differential equations before being numerically solved using the shooting method. Graphical results are shown in order to scrutinize the behavior of pertinent parameters on velocity, temperature profiles, and concentration of nanoparticle. Also, the behavior of fluid flow is investigated through the coefficient of the skin friction, Nusselt number, Sherwood number, and streamlines. Results showed that the velocity ratio parameter serves to increase the velocity of fluid and reduces the temperature distribution and nanoparticle concentration. The results were compared with the available studies and were found to be in excellent agreement.

Keywords

Carreau fluid, nanofluid, nonlinear thermal radiation, binary chemical reaction, activation energy, nonlinear stretching sheet

Date received: 12 December 2016; accepted: 2 February 2017

Introduction

The study of stagnation point flow due to stretching sheet that varies linearly or nonlinearly is a significant problem in engineering and has many applications in industries, dealing with polymer extrusion of sheets, cable coating, wire drawing, glass blowing, manufacturing of rubber and plastics sheets, melting spinning, hot rolling, and glass fiber production. In 1911, Hiemenz[1] first examined the steady flow near a stagnation point in moving fluid. Chiam[2] discussed the steady viscous flow near a stagnation point towards a stretching plate, and found that near the plate no boundary is formed when the velocities of stagnation flow and stretching plate are equal in the viscous free stream. Later on, this problem was reinvestigated by Mahapatra and Gupta[3] by taking different velocities of stagnation flow and stretching sheet. The boundary layer flow with heat and mass transfer towards a stagnation point past a stretching sheet with heat generation or absorption was scrutinized by Layek et al.[4] Nadeem et al.[5] discussed the boundary layer flow near a stagnation point over the stretching surface and obtained series solution using homotopy analysis method. Mousavi and Abbasbandy[6] investigated forced convective flow inside a circular tube embedded in Darcy–Brinkman–Forchheimer porous medium with heat flux. Seyf and Mousavi[7] obtained

[1]Department of Mathematical Sciences, Federal Urdu University of Arts, Science & Technology, Karachi, Pakistan
[2]Department of Civil Engineering, School of Engineering, University of Birmingham, Birmingham, UK
[3]Mechanical Engineering Department, Prince Mohammad Bin Fahd University, Saudi Arabia
[4]Department of Computational and Theoretical Sciences, Kulliyyah of Science, International Islamic University Malaysia, Kuantan, Malaysia

Corresponding author:
A Zaib, Department of Mathematical Sciences, Federal Urdu University of Arts, Science & Technology, Gulshan-e-Iqbal Karachi-75300, Pakistan.
Email: zaib20042002@yahoo.com

the analytical solution of boundary layer flow inside a permeable channel for Darcy–Brinkman equations with suction/injection. Shirazpour et al.[8] obtained the analytical solution of fully developed flow in a channel embedded in a Darcy–Brinkman porous medium with Lorentz force. Zaib and Shafie[9] investigated magnetohydrodynamic (MHD) viscous flow of a non-Newtonian fluid and heat with mass transfer near a stagnation point towards an unsteady stretching sheet. The effect of viscous dissipation in fluid flow embedded in a porous medium in the presence of nonlinear drag term bounded by two iso-flux or isothermal walls was investigated by Mousavi and Yaghoobi.[10] Bhattacharyya et al.[11] discussed the combined effects of Soret and Dufour on stagnation point flow over a shrinking sheet and obtained the dual solutions using the shooting method. Zaimi and Ishak[12] scrutinized the mixed convective flow on stagnation point towards a stretching sheet with partial slip effect and obtained the multiple solutions in the case of opposing flow. Recently, Awaludin et al.[13] performed the stability analysis of flow and heat transfer near a stagnation point over a stretching/shrinking sheet.

There are several fluids of engineering and industrial significance such as multigrade oils, blood polymers, petroleum production, composite material, fruit juices, and shampoos that display the viscoelastic behavior. These fluids cannot be described by simple model of Newtonian fluids. Due to the diversity of flow in nature, different non-Newtonian models have been suggested by researchers.[14,15] Among several models, one of the important non-Newtonian model is the Carreau fluid model, which is used frequently in chemical engineering. The Carreau fluids are generally identified as generalized Newtonian fluids, which are explained in detail by Bird et al.[16] The Carreau model fits the behavior of suspension of polymers in many fluid problems. It signifies the viscous fluid purely where the viscosity varies with the rate of deformation. Ali and Hayat[17] presented the analytical solution of the generalized Newtonian Carreau fluid of peristaltic motion in an asymmetric channel. The flow and heat transfer characteristics of Carreau fluid past a nonlinear stretching surface was examined by Khan and Hashim.[18] Recently, Khan et al.[19] obtained the numerical solution of the MHD flow of generalized Newtonian Carreau fluid past a heated stretching sheet with nonlinear thermal radiation. Very recently in the other paper, Khan et al.[20] scrutinized the MHD flow of a Carreau fluid near a stagnation point with heat transfer characteristics past a stretching sheet.

The process of mass transfer with binary chemical reaction and Arrhenius activation energy has been given a lot of attention due to its various applications in chemical engineering, cooling of nuclear reacting, geothermal reservoirs, and recovery of thermal oil. Generally, the relations between chemical reactions and mass transport are very complex, and can be scrutinized in the utilization of reactant species and production at several rates within the mass transfer and fluid. Bestman[21] was the first to consider the combined effects of the binary chemical reaction and Arrhenius activation energy on free convection flow with mass transfer in a vertical pipe immersed in a porous medium. He obtained the analytical solution using perturbation method. Maleque[22] studied the MHD free convection flow and heat with mass transfer over a porous vertical plate with binary chemical reaction and Arrhenius activation energy with heat generation\ absorption and viscous dissipation. In the other paper, Maleque[23] studied the MHD free convection flow over a permeable unsteady flat plate with exothermic/endothermic chemical reactions, Arrhenius activation energy, and thermal radiation. Mousavi et al.[24] investigated the viscous flow and heat transfer using two-equation energy model inside a channel embedded in porous medium. The unsteady flow with heat and mass transfer past a stretching sheet with binary chemical reaction with Arrhenius activation energy in a rotating fluid was scrutinized by Awad et al.[25] Recently, Shafique et al.[26] studied the steady flow of a non-Newtonian Maxwell fluid past an elastic surface in a rotating frame in the presence of binary chemical reaction along with the activation energy.

The aim of the current research is to scrutinize the combined effects of activation energy and binary chemical reaction along with nonlinear thermal radiation on stagnation point flow of a non-Newtonian (generalized Newtonian) Carreau fluid by dispersing nanoparticles towards a nonlinear stretching surface. The transmuted nonlinear ordinary differential equations are then numerically solved by using shooting method. To the best of the authors' knowledge, no one has yet considered this type of problem.

Mathematical formulation

Consider a steady two-dimensional stagnation point flow of a generalized Newtonian Carreau nanofluid past a nonlinear stretching sheet with activation energy and binary chemical reaction. The x-axis is taken along the stretching sheet in the direction of motion and the y-axis normal to it as shown in Figure 1. The variable stretching velocity is $u_w(x) = bx^m$ with $b > 0$ and $m > 0$ being constant and free stream velocity is $u_e(x) = dx^m$, where d is a positive constant towards a stagnation point from the sheet. Temperature T_w and concentration of nanoparticle C_w are taken as constants and the ambient temperature T_∞ and ambient concentration C_∞ are respectively taken as $y \to \infty$. The Brownian motion and thermophoresis effects are presented. Under these assumptions, the governing equations of motion, energy, and concentration of nanoparticle

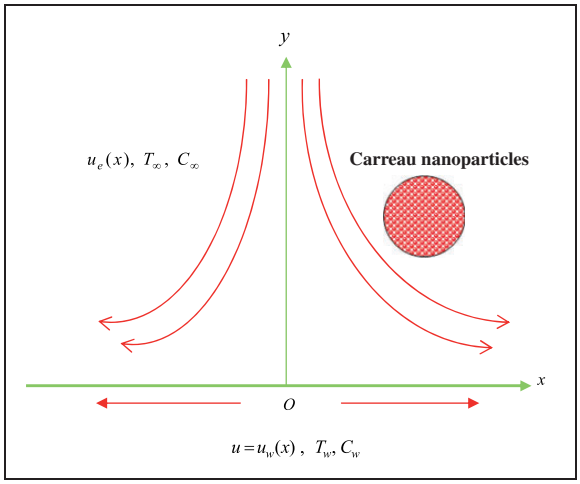

Figure 1. Flow diagram of the problem.

along with the boundary layer assumptions are written as

$$\frac{\partial u}{\partial x}+\frac{\partial v}{\partial y}=0 \tag{1}$$

$$u\frac{\partial u}{\partial x}+v\frac{\partial v}{\partial y}=u_e\frac{\mathrm{d}u_e}{\mathrm{d}x}+\nu\frac{\partial^2 u}{\partial y^2}\left[1+\Upsilon^2\left(\frac{\partial u}{\partial y}\right)^2\right]^{\frac{n-1}{2}} + \nu(n-1)\Upsilon^2\frac{\partial^2 u}{\partial y^2}\left(\frac{\partial u}{\partial y}\right)^2 \times\left[1+\Upsilon^2\left(\frac{\partial u}{\partial y}\right)^2\right]^{\frac{n-3}{2}} \tag{2}$$

$$u\frac{\partial T}{\partial x}+v\frac{\partial T}{\partial y}=\alpha_n\frac{\partial^2 T}{\partial y^2}+\tau\left[D_B\frac{\partial C}{\partial y}\frac{\partial T}{\partial y}+\left(\frac{D_T}{T_\infty}\right)\left(\frac{\partial T}{\partial y}\right)^2\right] -\frac{1}{(\rho c_p)_f}\frac{\partial q_r}{\partial y} \tag{3}$$

$$u\frac{\partial C}{\partial x}+v\frac{\partial C}{\partial y}=D_B\frac{\partial^2 C}{\partial y^2}+\left(\frac{D_T}{T_\infty}\right)\left(\frac{\partial^2 T}{\partial y^2}\right) -k_r^2\left(\frac{T}{T_\infty}\right)^{n_1}e^{-\frac{E_a}{\kappa T}}(C-C_\infty) \tag{4}$$

The appropriate boundary conditions are

$$\begin{aligned} &u=u_w(x), \quad v=0, \quad T=T_w, \quad C=C_w \quad \text{at } y=0\\ &u\to u_e(x), \quad T\to T_\infty, \quad C\to C_\infty \quad \text{as } y\to\infty \end{aligned} \tag{5}$$

where u and v are the components of velocity in x and y directions respectively, ν is the kinematic fluid viscosity, ρ is the density, Υ is the material constant called relaxation time, $\alpha_n=k/\rho c_p$ is the thermal diffusivity, c_p is the specific heat, k is the thermal conductivity, n is the power law index, T is the fluid temperature, T_∞ is the ambient temperature, C is the concentration of nanoparticle, D_B and D_T are the coefficients of Brownian and thermophoresis diffusion, respectively, τ is the ratio between the effective heat capacity of the nanoparticle material and specific heat capacitance of the fluid. It is worth mentioning that equation (2) can be reduced to Newtonian fluid when power law index $n=1$. Further, the value of power law index n in range $0<n<1$ and $n>1$ corresponds to the shear thinning and shear thickening behavior of fluids, respectively, $k_r^2(T/T_\infty)^{n_1}e^{-\frac{E_a}{\kappa T}}$ and κ are the modified Arrhenius function and the Boltzmann constant, respectively, where k_r^2 is the chemical reaction rate constant and n_1 is the fitted rate constant that lies between $-1<n_1<1$.

Following Khan et al.[19] the radiative heat flux q_r is expressed as

$$q_r=-\frac{4\sigma^*}{3k^*}\frac{\partial T^4}{\partial y} \tag{6}$$

where σ^* is the Stefan–Boltzmann constant and k^* is the mean absorption coefficient. It is noted that for a planer boundary layer flow past a hot plate, equation (6) further can be written as

$$q_r=-\frac{16\sigma^*}{3k^*}T^3\frac{\partial T}{\partial y} \tag{7}$$

Using equation (7), energy equation (3) can be written as

$$u\frac{\partial T}{\partial x}+v\frac{\partial T}{\partial y}=\frac{\partial}{\partial y}\left[\left(\alpha_n+\frac{16\sigma^*T^3}{3(\rho c_p)_f k^*}\right)\frac{\partial T}{\partial y}\right] +\tau\left[D_B\frac{\partial C}{\partial y}\frac{\partial T}{\partial y}+\left(\frac{D_T}{T_\infty}\right)\left(\frac{\partial T}{\partial y}\right)^2\right] \tag{8}$$

Introducing the following transformations

$$\begin{aligned} &\psi(x,y)=\sqrt{\frac{2\nu b}{m+1}}x^{(m+1)/2}f(\eta),\ \eta=y\sqrt{\frac{b(m+1)}{2\nu}}x^{(m-1)/2},\\ &\theta(\eta)=\frac{T-T_\infty}{T_w-T_\infty},\phi(\eta)=\frac{C-C_\infty}{C_w-C_\infty} \end{aligned} \tag{9}$$

Here η is the similarity variable, ψ is the stream function satisfying the continuity equation and is given in usual form as $u=\partial\psi/\partial y$ and $v=-\partial\psi/\partial x$. Here, we define the nondimensional temperature $\theta(\eta)=T-T_\infty/T_w-T_\infty$ with $T=T_\infty[1+(\theta_w-1)\theta]$ and $\theta_w>1$, where $\theta_w=T_w/T_\infty$ is the temperature ratio parameter. The first term on the right-hand side of equation (8) i.e. $\frac{\partial}{\partial y}\left[\alpha_n\frac{\partial T}{\partial y}+\frac{16\sigma^*T^3}{3(\rho c_p)_f k^*}\frac{\partial T}{\partial y}\right]$ can be further rewritten as $\frac{1}{\mathrm{Pr}}\theta''+\frac{4\mathrm{Pr}}{3N_d}\frac{d}{d\eta}[\{1+(\theta_w-1)\theta\}^3\theta']$, where $N_d=kk^*/4\sigma^*T_\infty^3$ is the thermal radiation parameter.

Using equation (9) and the above expression, the nonlinear partial differential equations (2), (4), and (8) are transmuted into the following nonlinear ordinary differential equations

$$\left\{1+nWe^2(f'')^2\right\}\left\{1+We^2(f'')^2\right\}^{\frac{n-3}{2}}f'''+ff''-\left(\frac{2m}{m+1}\right)\times\alpha^2=0 \tag{10}$$

$$\theta''+\Pr f\theta'+\frac{4}{3N_d}\frac{\mathrm{d}}{\mathrm{d}\eta}\left[\left\{1+(\theta_w-1)\theta\right\}^3\theta'\right]+\Pr Nb\theta'\phi'+\Pr Nt\theta'^2=0 \tag{11}$$

$$\phi''+Scf\phi'+\frac{Nt}{Nb}\theta''-\beta Sc(1+\delta\theta)^{n_1}\times\exp\left(-\frac{E}{1+\delta\theta}\right)\phi=0 \tag{12}$$

The converted boundary conditions

$$\left.\begin{array}{l} f(0)=0,\ f'(0)=1,\ \theta(0)=1,\ \phi(0)=1 \\ f'(\infty)\to\alpha,\ \theta(\infty)\to 0,\phi(\infty)\to 0 \end{array}\right\} \tag{13}$$

where prime denotes differentiation with respect to η, $We=\sqrt{b^3(m+1)\Upsilon^2x^{3m-1}/2\nu}$ is the local Weissenberg number, $\alpha=d/b$ is the ratio of velocity parameters, $\Pr=\nu/\alpha_n$ is the Prandtl number, $Nb=\tau D_B(C_w-C_\infty)/\nu$ is the Brownian motion parameter, $Nt=\tau D_T(T_w-T_\infty)/T_\infty\nu$ is the thermophoresis parameter, $E=E_a/\kappa T_\infty$ is the dimensionless activation energy, $\beta=k_r^2/bx^{m-1}$ is the nondimensional reaction rate, $\delta=(T_w-T_\infty)/T_\infty$ is the temperature difference parameter, and $Sc=\nu/D_B$ is the Schmidt number.

Quantities of physical interest are the local skin friction coefficient and the local Nusselt number, which are defined as

$$C_f=\frac{\eta_0}{\rho u_w^2}\left(\frac{\partial u}{\partial y}\left[1+\Upsilon^2\left(\frac{\partial u}{\partial y}\right)^2\right]^{\frac{n-1}{2}}\right),\quad Nu_x=-\frac{x}{k(T_w-T_\infty)}\left[-k\left(\frac{\partial T}{\partial y}\right)_w+(q_r)_w\right],\quad Sh_x=-\frac{x}{(C_w-C_\infty)}\left(\frac{\partial C}{\partial y}\right)_w \tag{14}$$

That is

$$C_f\mathrm{Re}_x^{1/2}=\sqrt{\frac{m+1}{2}}f''(0)\left[1+We^2(f''(0))^2\right]^{\frac{n-1}{2}}$$
$$Nu_x\mathrm{Re}_x^{-1/2}=-\sqrt{\frac{m+1}{2}}\theta'(0)\times\left\{1+\frac{4}{3N_d}[1+(\theta_w-1)\theta(0)]^3\right\},$$
$$Sh_x\mathrm{Re}_x^{-1/2}=-\sqrt{\frac{m+1}{2}}\phi'(0) \tag{15}$$

where $\mathrm{Re}_x=bx^{m+1}/\nu$ is the local Reynolds number.

Results and discussion

The transmuted nonlinear ordinary differential equations (10) to (12) associated with the boundary conditions (13) were numerically solved using the shooting method. The obtained numerical results for pertinent parameters involved in the problem are carried out through graphs and tables. Tables 1 and 2 display the comparison of our results of $f''(0)$ and $-\theta'(0)$ with the available results and show good agreement.

Figures 2 to 4 elucidate the behavior of velocity ratio parameter α on the velocity profile, temperature distribution, and concentration of nanoparticle. Figure 2 reveals that the larger values of velocity

Table 1. Comparison of $f''(0)$ when $n=1, We=0, m=1$ for several values of α.

α	Mahapatra and Gupta[27]	Ishak et al.[28]	Khan et al.[20]	Present
0.01	–	−0.9980	−0.998028	−0.9980
0.1	−0.9694	−0.9694	−0.969387	−0.9694
0.2	−0.9181	−0.9181	−0.918107	−0.9181
0.5	−0.6673	−0.6673	−0.667262	−0.6673
2.0	2.0175	2.0175	2.017487	2.0175
3.0	4.7293	4.7294	4.729260	4.7293

Table 2. Comparison of $-\theta'(0)$ when $n=1, We=0$, $m=1$, $N_d\to\infty, Nt=Nb=0$ for several values of Pr and α.

Pr	α	Mahapatra and Gupta[27]	Hayat[29]	Khan et al.[20]	Present
1	0.1	0.603	0.602156	0.602157	0.6022
	0.2	0.625	0.624467	0.624471	0.6245
	0.5	0.692	0.692460	0.692451	0.6925
1.5	0.1	0.777	0.776802	0.776807	0.7768
	0.2	0.797	0.797122	0.797129	0.7971
	0.5	0.863	0.864771	0.864806	0.8648

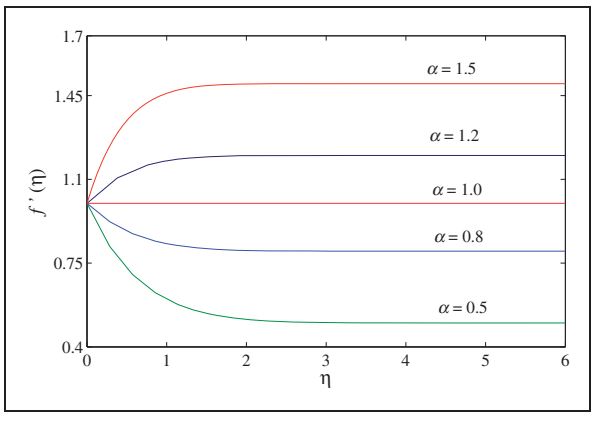

Figure 2. Velocity profile for different values of α when $We=2, n=0.8, m=1.5$.

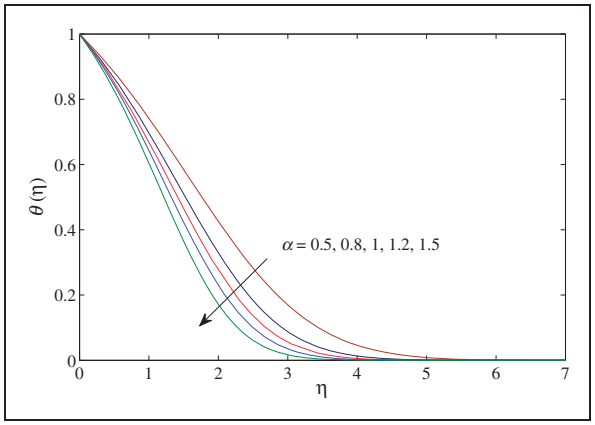

Figure 3. Temperature profile for different values of α when $We = 2, n = 0.8,\ m = 1.5, Nb = 1.5, Nt = 0.5,\ Q_w = 1.5,$ $N_d = 2,\ Pr = 1.$

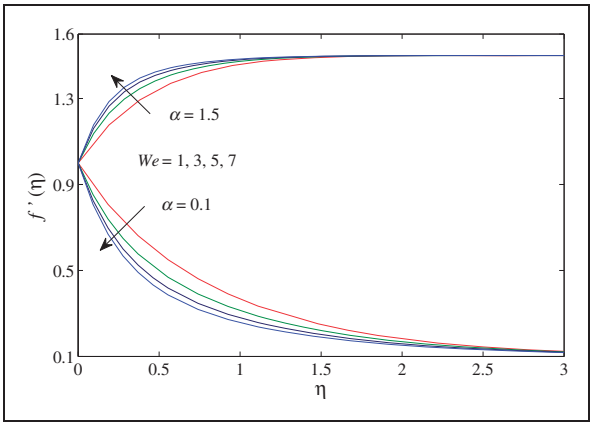

Figure 5. Velocity profile for different values of We when $n = 1.5, m = 1.5.$

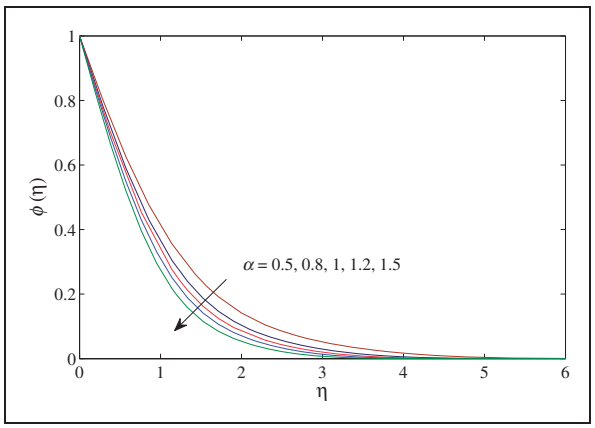

Figure 4. Concentration profile for different values of α when $We = 2, n = 0.8, m = 1.5, Nb = 1.5,\ Nt = 0.5,$ $Q_w = 1.5, N_d = 2,\ Pr = 1, \beta = 3, E = 6,\ n_1 = \delta = 0.5, Sc = 1.$

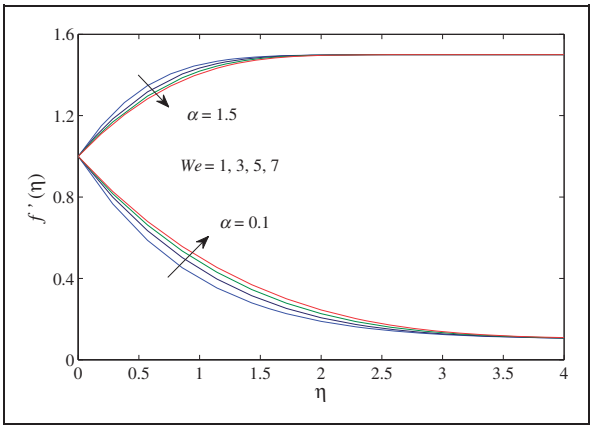

Figure 6. Velocity profile for different values of We when $n = 0.5, m = 1.5.$

ratio parameter α lead to increase in the velocity of fluid for both $\alpha < 1$ and $\alpha > 1$, whereas the thickness of momentum boundary layer shows the reverse trend in both cases. Physically, the value of α indicates the ratio of stretching to free stream velocities. Increase in the value of α implies that the velocity of free stream is larger than the velocity of stretching sheet. As observed by Mahapatra and Gupta,[27] the value of b implies stretching sheet and enhancement in a relation to b_{causes} an increase in the motion of strain towards a region of stagnation point, which can increase the acceleration of the external stream. However, when the velocity is larger than the velocity of free stream $\alpha < 1$, the flow elucidates a reversed structure of boundary layer and, consequently, the thickness of boundary layer enhances with an increase in α for $\alpha < 1$. On the other hand, temperature distribution and concentration of nanoparticle reduce due to velocity ratio parameter as shown in Figures 3 and 4, respectively. Thus, the thermal and concentration boundary layer thicknesses become thinner and thinner for larger values of α.

The impact of Weissenberg number We on the velocity profile for shear thickening ($n > 1$) and shear thinning ($n < 1$) fluids are specified in Figures 5 and 6, respectively. Figure 5 shows that for shear thickening fluid the velocity of fluid decreases with larger values of We and thickness of momentum boundary layer increases for $\alpha > 1$. While in the case of $\alpha < 1$, the velocity and the momentum boundary layer thickness enhance with higher values of We. On the other hand, the reverse outcome is observed for shear thinning fluid in both cases of $\alpha < 1$ and $\alpha > 1$ as shown in Figure 6. Physical reason behind that is the fluids are more viscous in case of shear thickening compared to shear thinning fluid or Newtonian fluid, which causes the slowdown of the motion and, thus, velocity of the fluid decreases.

Figures 7 and 8 depict the impact of thermophoresis parameter Nt on the temperature distribution and concentration of nanoparticle, respectively. The figures specify that the temperature distribution as well as the concentration of nanoparticle increase by uplifting Nt for $\alpha < 1$ and $\alpha > 1$. This is because diffusion penetrates deeper into the fluid due to

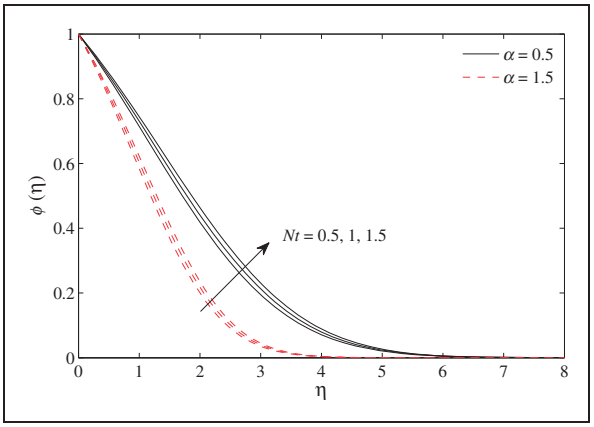

Figure 7. Temperature profile for different values of Nt when $We = 2, m = 2, n = 1.5 Nb = 1, Q_w = 1.2, N_d = 1,\ Pr = 1$.

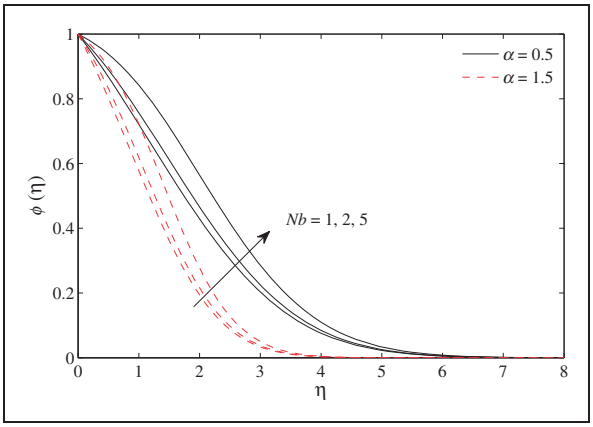

Figure 9. Temperature profile for different values of Nb when $We = 2, m = 2, Nt = 0.5, Q_w = 1.2, N_d = 1,\ Pr = 1$.

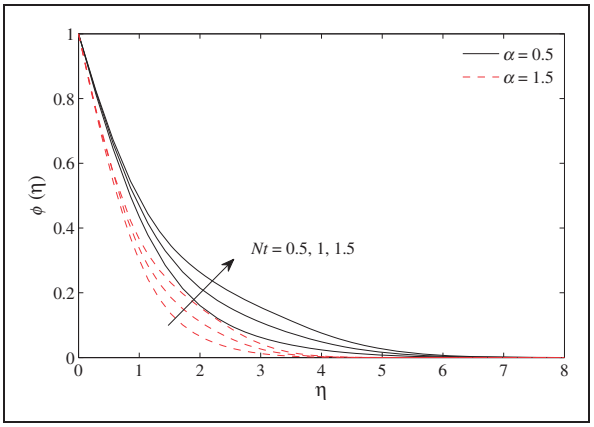

Figure 8. Concentration profile for different values of Nt when $We = 2, m = 2, n = 1.5, Nb = 1.5, Q_w = 1.2, N_d = 1,\ Pr = 1, \beta = 2, E = 10, n_1 = \delta = 0.5, Sc = 1$.

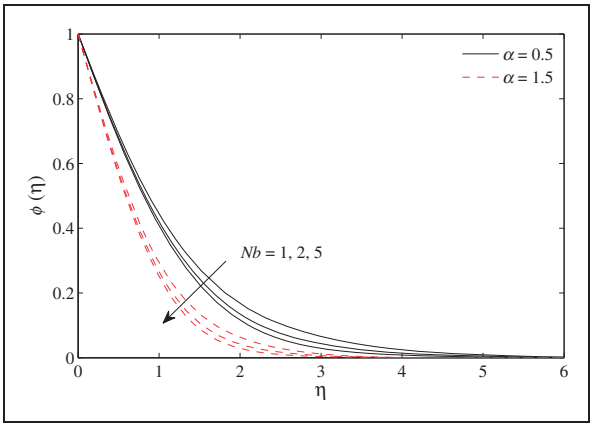

Figure 10. Concentration profile for different values of Nb when $We = 2, m = 2, Nt = 0.5, Q_w = 1.2, N_d = 1,\ Pr = 1, \beta = 2, E = 10, n_1 = \delta = 0.5, Sc = 1$.

increasing values of Nt, which causes the thickening of the thermal boundary layer as well as the concentration boundary layer. It is interesting to note that the effect of thermophoresis parameter is more pronounced on the concentration of nanoparticle compared to the temperature distribution. Further, the temperature profile and concentration of nanoparticle have larger impact in the case of $\alpha < 1$ compared to $\alpha > 1$.

Figures 9 and 10 are prepared to see the Brownian motion effect Nb on the temperature distribution and concentration of nanoparticle, respectively. Figure 9 elucidates that the temperature distribution and thermal boundary layer thickness enhance with larger values of Nb. Physical reason is that the kinetic energy of the nanoparticle increases due to the strength of this chaotic motion and as a result the fluid's temperature increases, whereas the opposite trend is seen on the concentration nanoparticle as depicted in Figure 10. It can be seen that the concentration nanoparticle decreases due to the increasing values of Nb. It can be concluded that the Brownian

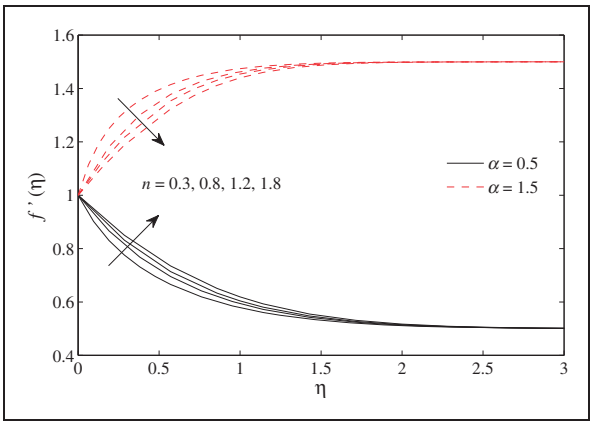

Figure 11. Velocity profile for different values of n when $We = 2, m = 2$.

motion parameter makes the fluid warm within the boundary and at that time aggravates deposition particles away from the regime of fluid to the surface that causes a decrease in the concentration profile as well

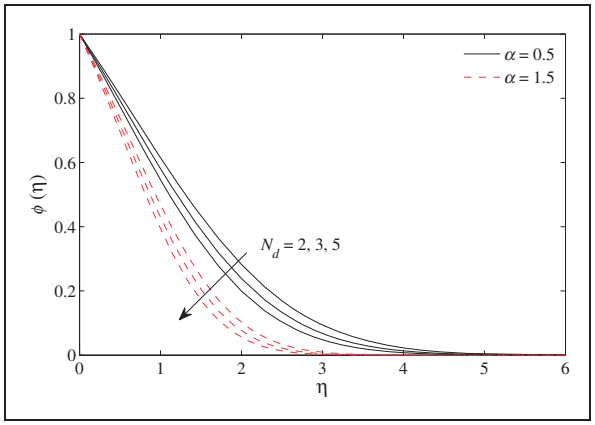

Figure 12. Temperature profile for different values of N_d when $We = 2, m = 2,\ Nt = 0.2, Nb = 0.2, Q_w = 1.2,$ $n = 1.5,\ Pr = 1.$

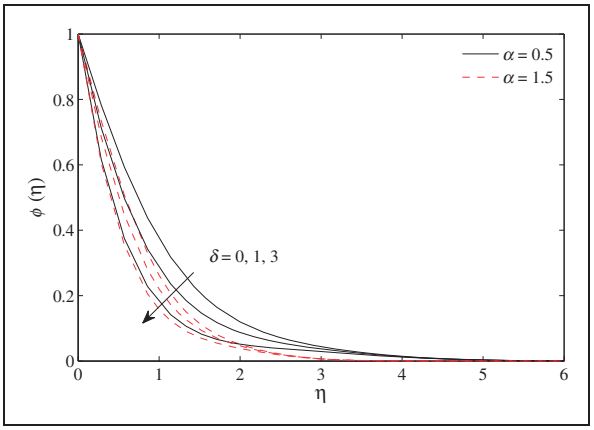

Figure 15. Concentration profile for different values of δ when $We = 2, m = 2, Nt = 0.5, Nb = 0.5, Q_w = 1.5,$ $n = 1.5,\ Pr = 1, \beta = 5,\ E = 3, n_1 = 0.5, Sc = 1.$

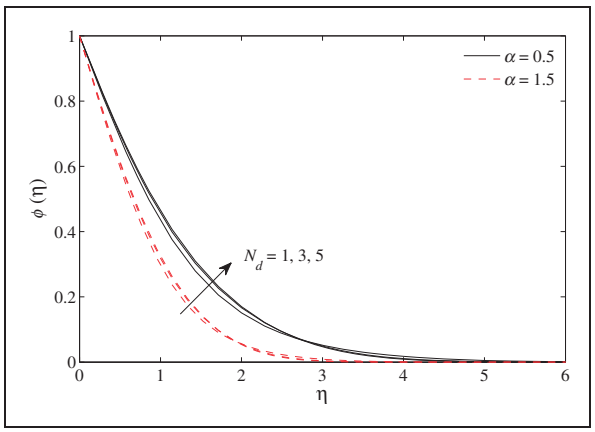

Figure 13. Concentration profile for different values of N_d when $We = 2, m = 2, Nt = 0.2,\ Nb = 0.2, Q_w = 1.2,$ $n = 1.5,\ Pr = 1, \beta = 2, E = 10, n_1 = \delta = 0.5, Sc = 1.$

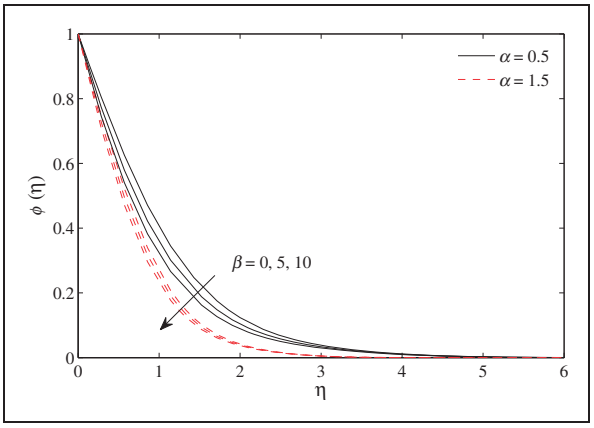

Figure 16. Concentration profile for different values of β when $We = 2, m = 2, Nt = 0.5, Nb = 2.5, Q_w = 1.5, n = 1.5,$ $Pr = 1, \delta = 0.5,\ E = 4, n_1 = 0.5, Sc = 1.$

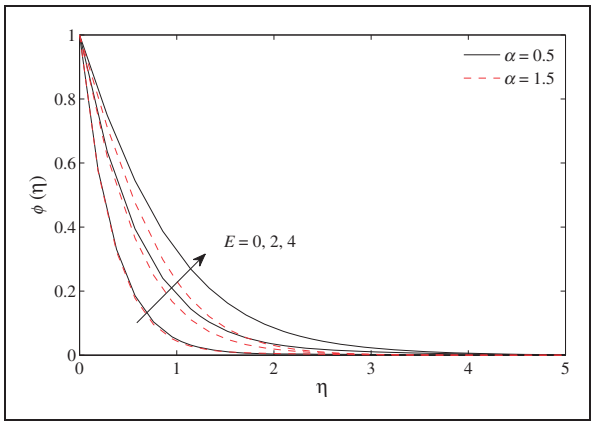

Figure 14. Concentration profile for different values of E when $We = 2, m = 2, Nt = 0.2, Nb = 1.5, Q_w = 1.5,$ $n = 1.5,\ Pr = 1, \beta = 10,\ \delta = 0.5, n_1 = 0.3, Sc = 1.$

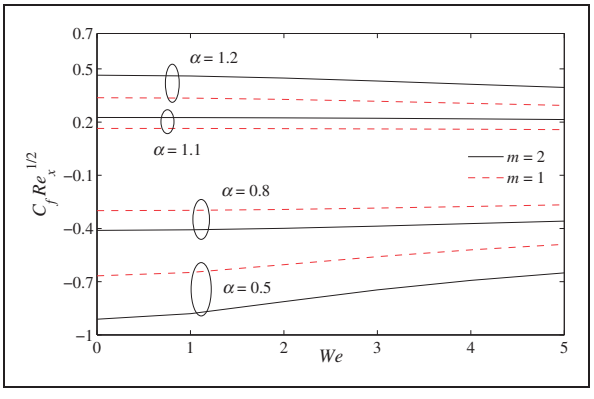

Figure 17. Skin friction versus We for various values of α when $n = 0.5$.

as the thickness of boundary layer. The larger values of Brownian motion imply the strong behavior for the smaller particle, whereas for stronger particle the smaller values of Nb are applied.

Figure 11 elucidates the behavior of power law index n on the velocity profile for both cases of $\alpha < 1$ and $\alpha > 1$. This figure reveals that in the case of $\alpha < 1$ the velocity of fluid and the thickness of momentum boundary layer enhance due to larger

values of power law index n, whereas in case of $\alpha > 1$ the contraction is seen in fluid velocity due to higher values of n. Thus, power law index plays an important role in the structure of boundary layer. The behavior of temperature distribution and concentration of nanoparticle for various values of nonlinear radiation parameter N_d are demonstrated in Figures 12 and 13, respectively. Figure 12 signifies a decreasing behavior for increasing values of N_d. Thus, the thermal boundary layer thickness becomes thinner and thinner while the nanoparticle concentration and boundary thickness concentration enhance with larger values of N_d as shown in Figure 13. This is due to the fact that a large value of the radiation parameter implies the dominance of conduction and, therefore, the thermal boundary layer thickness reduces and concentration boundary layer thickness increases. The effect of radiation parameter is more pronounced on the temperature distribution compared to the nanoparticle concentration. Further, the profiles of temperature distribution and concentration nanoparticle are larger for $\alpha < 1$ compared to $\alpha > 1$.

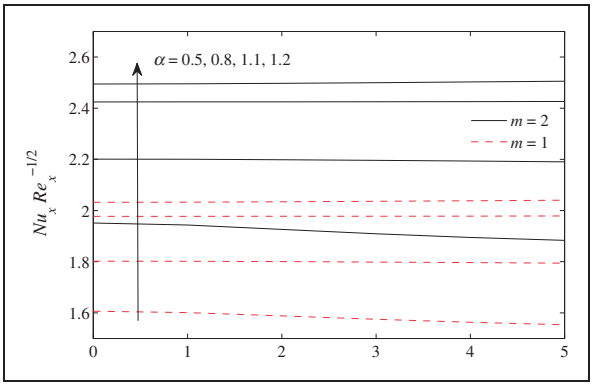

Figure 18. Nusselt number versus *We* for various values of α when $Nb = 1.2, n = 0.5, Nt = 0.5, Q_w = 1.2, N_d = 2,\ Pr = 1$.

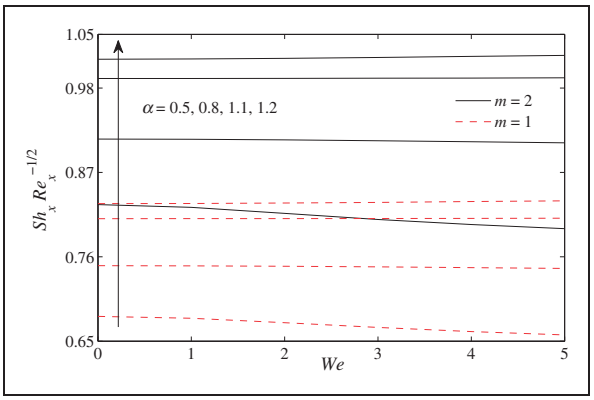

Figure 19. Sherwood number versus *We* for various values of α when $Nt = 0.2, Nb = 1.2, Q_w = 1.2, n = 0.5,\ N_d = 2,$ $Pr = 1, \beta = 2,\ \delta = 0.5,\ E = 10, n_1 = 0.5, Sc = 1$.

Figure 14 elucidates the increasing behavior in concentration profile due to increasing values of nondimensional activation energy E and leads to the increase in the concentration of boundary layer thickness. Physically, higher activation energy and lower temperature leads to lesser reaction rate, which slows down the chemical reaction. Figure 15 preserves the influence of temperature difference δ on the concentration profile. This result showed that the concentration profile and concentration boundary layer thickness decrease due to increasing values of δ. Figure 16 shows that due to increase in the values of dimensionless reaction rate β, the concentration profile decreases and results in the thinning of the concentration boundary layer thickness. Physically, an increase in the value of β leads to an increase in the term $\beta(1+\delta\theta)^n \exp(-E/1+\delta\theta)$. This ultimately helps the destructive chemical reaction that increases the concentration.

Table 3. The values of skin friction, Nusselt number, and Sherwood number for various values of linear and nonlinear stretching sheets α when $n = 0.5, N_d = 2,\ Nt = 0.2, Nb = 1.2,\ Pr = 1,\ Q_w = 1.2, \beta = 2, E = 10, n_1 = \delta = 0.5, Sc = 1$.

		$C_f \mathrm{Re}_x^{1/2}$		$Nu_x \mathrm{Re}_x^{-1/2}$		$Sh_x \mathrm{Re}_x^{-1/2}$	
α	*We*	$m_1 = 1$	$m_2 = 2$	$m_1 = 1$	$m_2 = 2$	$m_1 = 1$	$m_2 = 2$
0.5	0	−0.6673	−0.9119	1.6067	1.9512	0.6824	0.8281
	1	−0.6480	−0.8804	1.6012	1.9434	0.6799	0.8245
	3	−0.5588	−0.7462	1.5749	1.9091	0.6680	0.8087
0.8	0	−0.2994	−0.4106	1.8019	2.2009	0.7484	0.9135
	1	−0.2976	−0.4076	1.8015	2.2003	0.7482	0.9132
	3	−0.2848	−0.3867	1.7986	2.1962	0.7469	0.9113
1.1	0	0.1643	0.2259	1.9773	2.4246	0.8097	0.9925
	1	0.1640	0.2254	1.9774	2.4247	0.8098	0.9925
	3	0.1617	0.2215	1.9778	2.4253	0.8100	0.9928
1.2	0	0.3377	0.4646	2.0324	2.4946	0.8293	1.0175
	1	0.3352	0.4603	2.0328	2.4953	0.8295	1.0179
	3	0.3177	0.4316	2.0360	2.4997	0.8309	1.0199

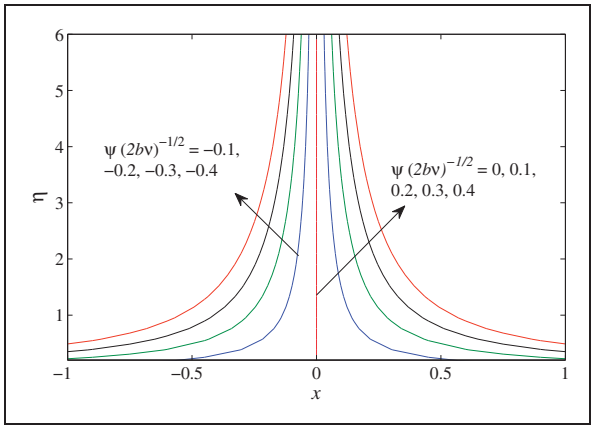

Figure 20. Streamlines for two-dimensional flow when $We = 2, m = 2, n = 0.5, \alpha = 0.5$.

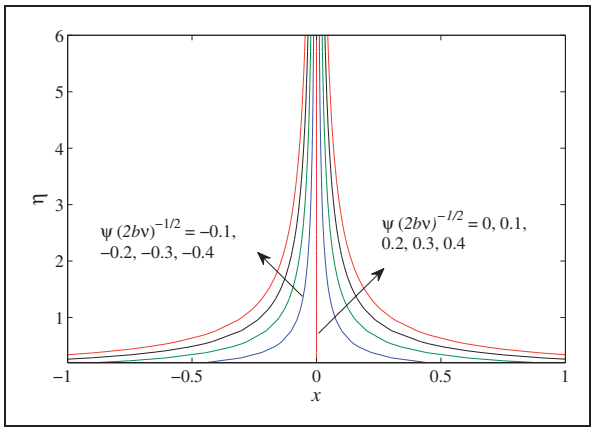

Figure 21. Streamlines for two-dimensional flow when $We = 2, m = 2, n = 0.5, \alpha = 1.5$.

The impact of velocity ratio parameter versus We on the skin friction, Nusselt number, and Sherwood number are presented in Figures 17 to 19 for linear $(m = 1)$ and nonlinear $(m \neq 1)$ stretching sheets. Figure 17 shows that the value of skin friction leads to enhancement as the velocity ratio increases for both linear and nonlinear stretching sheets. However, the values of the skin friction increases with increasing We in case of $\alpha < 1$ whereas the values decreases when $\alpha > 1$. It is interesting to see from this figure that the values of skin friction is higher for the nonlinear stretching sheet compared to the linear stretching sheet when $\alpha > 1$, whereas the reverse trend is seen when $\alpha < 1$. On the other hand, the Nusselt number and the Sherwood number increase for linear and nonlinear stretching sheets as shown in Figures 18 and 19, respectively. The values are more pronounced for nonlinear stretching sheet when compared to linear stretching sheet. The behavior is also shown in Table 3.

Finally, the sketch of streamlines using stream function ψ are illustrated in Figures 20 and 21 for both cases of $\alpha < 1$ and $\alpha > 1$, respectively. These figures signify that streamlines are moderately simple, symmetric, and fuller towards an axis because of the equal force moving in the opposite direction, which causes the sheet to enlarge. Similar pattern is observed when $\alpha > 1$ but the streamlines are squeezed.

Conclusion

In this research, we explored the physical features of generalized Newtonian Carreau fluid immersed in nanofluid near a stagnation point towards a nonlinear stretching sheet with nonlinear thermal radiation. Further, we considered the combined effects of binary chemical reaction with activation energy. The transmuted ordinary differential equations were numerically solved using the shooting method. Some significant features of the problem regarding the various pertinent parameters were gathered. The velocity boundary layer become thicker when the velocity of stretching sheet dominates the velocity of free stream $(\alpha < 1)$, whereas a reverse effect was seen when the velocity of free stream dominates the velocity of stretching sheet $(\alpha > 1)$. On the other hand, temperature of fluid as well as the concentration of nanoparticle decline as the velocity ratio increases. We observed that the Weissenberg number has relatively reverse effect on the fluid velocity in case of two different velocity ratio parameters. Strength of the thermophoresis parameter enhanced the temperature distribution as well as the concentration of nanoparticle for both $\alpha < 1$ and $\alpha > 1$. Brownian motion strengthens the temperature profile and weaken the concentration of nanoparticle. Large value of the radiation parameter reduces the thermal boundary layer thickness and enhances the concentration boundary layer thickness. Temperature difference parameter and dimensionless reaction parameter reduce the concentration profile, whereas the profile enhances due to activation energy parameter. The values of skin friction are higher for nonlinear stretching sheet compared to linear stretching sheet when $\alpha > 1$, while an opposite trend is perceived when $\alpha < 1$.

Acknowledgement

The authors are very thankful to the editor and the reviewers for their valuable comments that helped in improving the presentation of this paper.

Declaration of Conflicting Interests

The author(s) declared no potential conflicts of interest with respect to the research, authorship, and/or publication of this article.

Funding

The author(s) received no financial support for the research, authorship, and/or publication of this article.

References

1. Hiemenz K. Die Grenzschicht an einem in den gleichformingen Flussigkeitsstrom einge-tauchten graden Kreiszylinder. *Dinglers Polytech J* 1911; 326: 321–324.

2. Chiam TC. Stagnation-point flow towards a stretching plate. *J Phys Soc Jpn* 1994; 63: 2443–2444.
3. Mahapatra TR and Gupta AS. Magnetohydrodynamic stagnation-point flow towards a stretching sheet. *Acta Mech* 2001; 152: 191–196.
4. Layek GC, Mukhopadhyay S and Samad SkA. Heat and mass transfer analysis for boundary layer stagnation-point flow towards a heated porous stretching sheet with heat absorption/generation and suction/blowing. *Int Commun Heat Mass Transfer* 2007; 34: 347–356.
5. Nadeem S, Hussain A and Khan M. HAM solutions for boundary layer flow in the region of the stagnation point towards a stretching sheet. *Commun Nonlinear Sci Numer Simul* 2010; 15: 475–481.
6. Mousavi SMR and Abbasbandy S. Analysis of forced convection in a circular tube filled with a Darcy-Brinkman-Forchheimer porous medium using spectral homotopy analysis method. *ASME J Fluids Eng* 2011; 133: 101207.
7. Seyf HR and Mousavi SMR. An analytical study for fluid flow in porous media imbedded inside a channel with moving or stationary walls subjected to injection/suction. *ASME J Fluids Eng* 2001; 133: 091203.
8. Shirazpour A, Mousavi SMR and Seyf HR. HPM solution of momentum equation for Darcy-Brinkman model in a parallel plates channel subjected to Lorentz force. In: *International conference on fluid mechanics, heat transfer and thermodynamics*, Amsterdam, Netherlands, 13–15 July 2013, 2011, pp.258–262.
9. Zaib A and Shafie S. Unsteady MHD stagnation-point flow with heat and mass transfer in a micropolar fluid in the presence of thermophoresis and suction/injection. *Indian J Pure Appl Math* 2013; 44: 1–18.
10. Mousavi SMR and Yaghoobi H. Effect of non-linear drag term on viscous dissipation in a fluid saturated porous medium channel with various boundary conditions at walls. *Arabian J Sci Eng* 2014; 39: 1231–1240.
11. Bhattacharyya K, Layek GC and Seth GS. Soret and Dufour effects on convective heat and mass transfer in stagnation-point flow towards a shrinking surface. *Phys Scr* 2014; 89: 095203.
12. Zaimi K and Ishak A. Stagnation-point flow towards a stretching vertical sheet with slip effects. *Mathematics* 2016; 4: 1–8.
13. Awaludin IS, Weidman PD and Ishak A. Stability analysis of stagnation-point flow over a stretching/shrinking sheet. *AIP Adv* 2016; 6: 045308.
14. Mousavi SMR, Abbasbandy S and Alsulami HH. Analytical flow study of a conducting Maxwell fluid through a porous saturated channel at various wall boundary conditions. *Eur Phys J Plus* 2014; 129: 1–10.
15. Zaib A, Bhattacharyya K, Uddin Md S, et al. Dual solutions of non-Newtonian Casson fluid flow and heat transfer over an exponentially permeable shrinking sheet with viscous dissipation. *Model Simul Eng* 2016; 2016: 1–8.
16. Bird RB, Curtiss CF, Armstrong RC, et al. *Dynamics of polymeric liquids*. New York: Wiley, 1987.
17. Ali N and Hayat T. Peristaltic motion of a Carreau fluid in an asymmetric channel. *Appl Math Comput* 2007; 193: 535–552.
18. Khan M and Ali H. Boundary layer flow and heat transfer to Carreau fluid over a nonlinear stretching sheet. *AIP Adv* 2015; 5: 1–14.
19. Khan M, Ali H, Hussain M, et al. Magnetohydrodynamic flow of Carreau fluid over a convectively heated surface in the presence of non-linear radiation. *J Magnet Mag Mat* 2016; 412: 63–68.
20. Khan M, Ali H and Alshomrani AS. MHD stagnation-point flow of a Carreau fluid and heat transfer in the presence of convective boundary conditions. *Plos One* 2016; 11: e0157180.
21. Bestman AR. Natural convection boundary layer with suction and mass transfer in a porous medium. *Int J Eng Res* 1990; 14: 389–396.
22. Maleque KhA. Effects of binary chemical reaction and activation energy on MHD boundary layer heat and mass transfer flow with viscous dissipation and heat generation/absorption. *ISRN Thermodyn* 2013; 2013: 1–9.
23. Maleque KhA. Effects of exothermic/endothermic chemical reactions with Arrhenius activation energy on MHD free convection and mass transfer flow in presence of thermal radiation. *J Thermodyn* 2013; 2013: 1–11.
24. Mousavi SMR, Seyf HR and Abbasbandy S. Heat transfer through a porous saturated channel with permeable walls using two-equation energy model. *J Porous Media* 2013; 16: 241–254.
25. Awad FG, Motsa S and Khumalo M. Heat and mass transfer in unsteady rotating fluid flow with binary chemical reaction and activation energy. *Plos One* 2014; 9: 1–12.
26. Shafique Z, Mustafa M and Mushtaq A. Boundary layer flow of Maxwell fluid in rotating frame with binary chemical reaction and activation energy. *Results Phys* 2014; 6: 1–7.
27. Mahapatra TR and Gupta AG. Heat transfer in stagnation point flow towards a stretching sheet. *Heat Mass Transfer* 2002; 38: 517–521.
28. Ishak A, Nazr R and Pop I. Mixed convection boundary layers in the stagnation-point flow toward a stretching vertical sheet. *Meccanica* 2006; 41: 509–518.
29. Hayat T, Javed T and Abbas Z. MHD flow of a micropolar fluid near a stagnation-point towards a non-linear stretching surface. *Non-Linear Anal Real World Appl* 2009; 10: 1514–1526.

Appendix

Notation

b, d, m	positive constants
C_f	skin friction coefficient
C	concentration of nanoparticle
C_w	concentration of nanoparticle at the surface
C_∞	ambient concentration of nanoparticles
D_B	coefficient of Brownian diffusion ($m^2 \cdot s^{-1}$)
D_T	coefficient of thermophoresis diffusion ($m^2 \cdot s^{-1}$)
E_a	activation energy
E	dimensionless activation energy
f	dimensionless stream function
k	thermal conductivity ($W \cdot m^{-1} K^{-1}$)

k_r^2	chemical reaction rate constant
k^*	mean absorption coefficient
m_w	mass flux
n	power law index
n_1	fitted rate constant
Nb	Brownian motion parameter
Nt	thermophoresis parameter
Nu_x	Nusselt number
Pr	Prandtl number
q_r	radiative heat flux (kg m^{-1} s^{-3} K^{-1})
q_w	heat flux ($W{\cdot}m^{-2}$)
Re_x	local Reynolds number
N_d	thermal radiation parameter
Sc	Schmidt number
Sh_x	Sherwood number
T	temperature (K)
T_∞	free stream temperature (K)
T_w	fluid temperature at wall (K)
u_e	free stream velocity ($m{\cdot}s^{-1}$)
u, v	velocity components ($m{\cdot}s^{-1}$)
We	local Weissenberg number
x, y	Cartesian coordinates (m)
α	ratio of velocity parameters
α_n	thermal diffusivity ($m^2\,s^{-1}$)
β	dimensionless reaction rate
δ	temperature difference parameter
η	similarity variable
Υ	material constant called relaxation time
κ	Boltzmann constant
ν	kinematic viscosity ($m^2{\cdot}s^{-1}$)
ϕ	dimensionless concentration of nanoparticle
ψ	stream function
ρ	density ($kg{\cdot}m^{-3}$)
$(\rho c_p)_f$	specific heat capacitance of nanofluid ($J{\cdot}m^{-3}{\cdot}K^{-1}$)
$(\rho c_p)_p$	effective heat capacitance of nanofluid ($J{\cdot}m^{-3}{\cdot}K^{-1}$)
σ^*	Stefan–Boltzmann constant [$kg\,s^{-3}\,K^{-4}$]
τ	ratio of heat capacitance ($J{\cdot}K^{-1}$)
τ_w	shear stress at the surface ($N{\cdot}m^{-2}$)
θ	dimensionless temperature
θ_w	temperature ratio parameter

Subscript

w	condition at wall
∞	condition at free stream

Superscript

$'$	derivative w.r.t. η